THE JOURNAL OF PHYSICAL CHEMISTRY C

Article

pubs.acs.org/JPCC

Zinc Electrodeposition on Polycrystalline Copper: Electrochemical Study of Early-Stage Growth Mechanism

Shaohui Xu,*[,†,‡,§] Yiping Zhu,[†] Dayuan Xiong,[†,‡] Lianwei Wang,[†] Pingxiong Yang,[†] and Paul K. Chu[§]

[†]Key Laboratory of Polar Materials and Devices, Ministry of Education, and Department of Electronic Engineering, East China Normal University, 500 Dongchuan Road, Minhang District, Shanghai 200241, China

[‡]Shanghai Key Laboratory of Multidimensional Information Processing, East China Normal University, Shanghai 200241, China

[§]Department of Physics and Materials Science, City University of Hong Kong, Tat Chee Avenue, Kowloon, Hong Kong, China

ABSTRACT: The early stage growth mechanism of zinc clusters electrodeposited on polycrystalline copper is studied by electrochemical methods. By analyzing the chronoamperometric and chronocoulometric data, nucleation and growth of the Zn layer as a function of time are investigated, and a growth model is proposed and discussed. Experimental and theoretical details about chronocoulometric data reveal a three-step growth mechanism. The results provide insights into the mechanism of electrodeposition of metallic particles. The same analysis process can also be described as the stripping mechanism. The formation and stripping mechanisms of a zinc adlayer can be predicted considering the contribution of four-different processes: a Langmuir-type adsorption/desorption process, the two-dimensional nucleation and growth in instantaneous and progressive cases, and a three-dimensional nucleation and growth process under diffusion-limited condition.

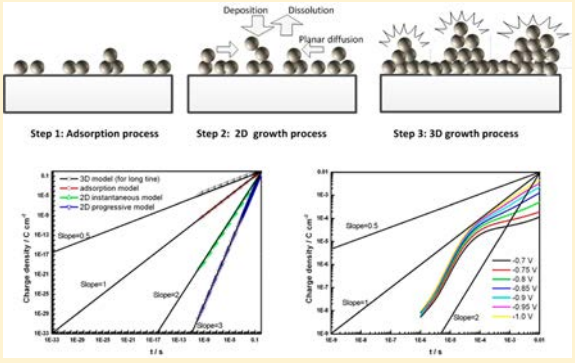

1. INTRODUCTION

Because of their unique properties of nanoscale materials as compared to their bulk counterparts and tunable properties by size and shape adjustment, metallic nanocrystals have gained much attraction in different fields such as catalysis and sensing.[1−5] Metal nanocrystals can be synthesized by several methods[2] such as colloidal synthesis, sol−gel deposition, hydrothermal synthesis, vapor deposition, and electrochemical deposition. In particular, electrochemical deposition, which can produce metallic nanostructures in one step without extensive sample preparation, is surfactant free and cost-effective, and the properties of the nanocrystals can be changed by adjusting the electrolyte and deposition parameters. It has been used to prepare high-quality metallic nanoparticles such as Pt, Pb, and Te on different substrates for fuel cells and sensing devices.[6−10] Despite recent advances, it is still challenging to prepare metal nanoparticles with tunable size- and shape-dependent properties, especially nanoparticles with narrow size distributions. Therefore, it is important to understand the nucleation and growth mechanism during metal electrodeposition. Because the formation of the initial monolayer is critical to the structure of the deposited layer,[11,12] the early stages in electrodeposition must be better understood. New knowledge about the kinetics of initial monolayer formation will expedite application to catalysis and corrosion resistance as well as disclose the formation dynamics of self-assembled thin films.

Metal electrodeposition has been studied both theoretically and experimentally. The theoretical model developed by Scharifker et al.[13,14] and developed by others[15−23] shows that electrochemically formed nuclei grow by direct reduction of ions onto the surface affecting both the concentration of active species and the overpotential distribution in the cluster vicinity to create zones with a reduced concentration and consequently smaller nucleation rate. If multiple clusters are considered, the local zones with a reduced nucleation rate spread and overlap gradually. Electrochemical nucleation and growth have traditionally been evaluated indirectly by measuring the current−time transients in potentiostatic experiments and correlating them to models that take into account the random nature of nucleation and coupled growth of hemispherical nuclei under diffusion limitations. Eectrodeposition of silver or Pt nanoparticles has been investigated by aberration-corrected and high-angle annular dark-field scanning transmission electron microscopy (HAADF-STEM).[24] The actual particle size distribution and atomic scale structural information can be correlated with electrochemical measurements, enabling better understanding of the early stages in electrochemical nanoparticle formation. In fact, an electrochemical aggregative growth mechanism[25,26] has been proposed to achieve the right balance between nucleation, self-limiting growth, cluster surface diffusion, coalescence, and morphology of the nanostructures. However, it is still necessary to obtain more information about the mechanism by chronoamperometry and chronocoulometry. This is the objective of this piece of work so that

Received: November 30, 2016
Revised: January 19, 2017
Published: January 20, 2017

ACS Publications © 2017 American Chemical Society

DOI: 10.1021/acs.jpcc.6b12036
J. Phys. Chem. C 2017, 121, 3938−3946

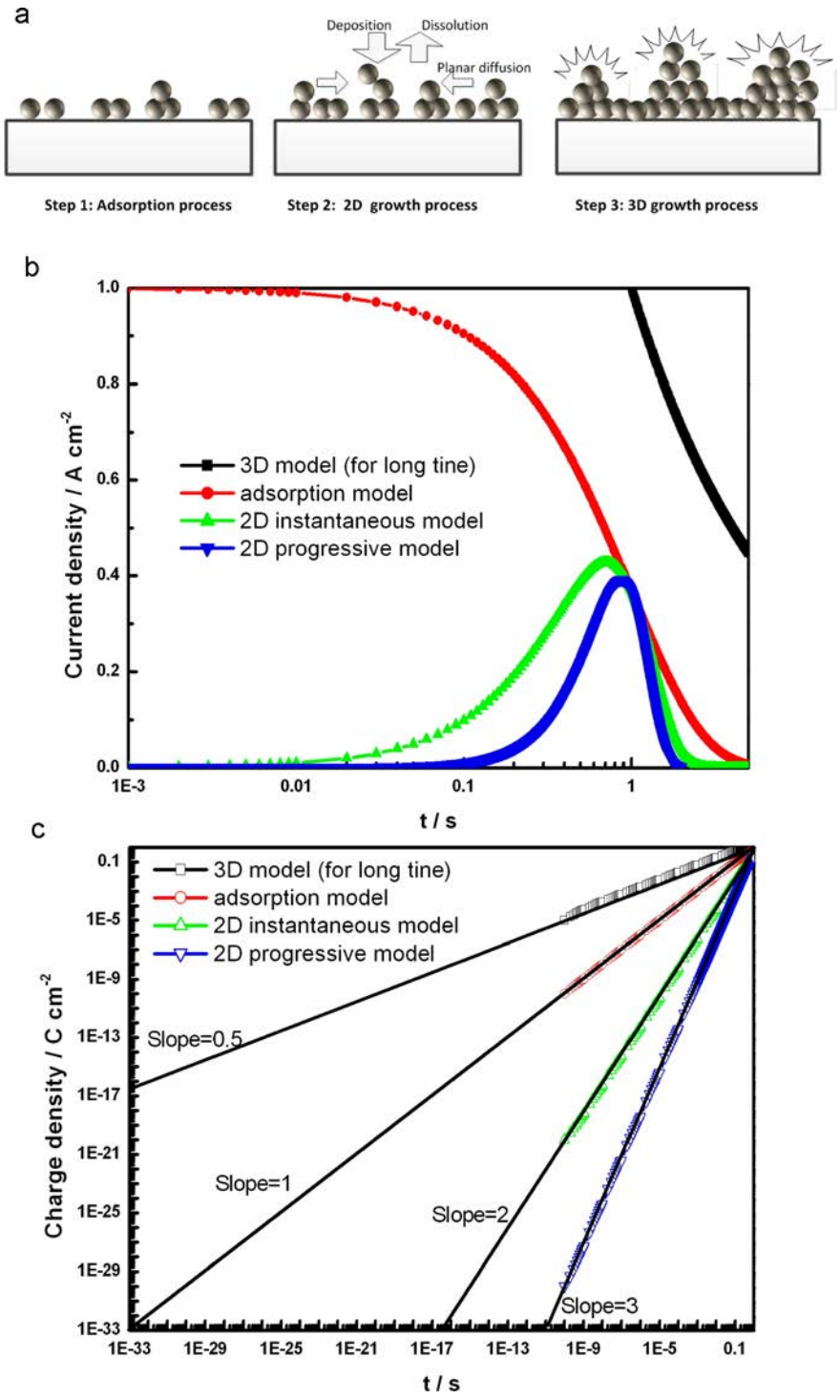

Figure 1. (a) Schematic illustration of the growth mechanism of the electrodeposition process; and (b) current and (c) charge densities versus time calculated by the growth model. The adjusted parameters are unity for simplicity, and solid lines with slopes of 0.5, 1, 2, and 3 are shown for comparison.

electrochemical deposition can be used more conveniently to produce nanostructures with the desired morphology as well as enhanced properties.

2. EXPERIMENTAL DETAILS

A polycrystalline copper sheet (99.99% pure) served as the working electrode in the experiments. After grinding with sandpaper, the copper electrodes were cleaned with acetone and then deionized water ultrasonically for 10 min. The electrochemical experiments were carried out on a three-electrode electrochemical working station (Shanghai Chenhua CHI660D) in 1 mol L^{-1} aqueous $ZnBr_2$ solution with the saturated calomel electrode (SCE) and platinum electrode being the reference electrode and counter electrode, respectively. Cyclic voltammetry (CV) was performed in the potential range between −1.2 and −0.6 V versus SCE at scanning rates between 10 and 200 mV s^{-1}. Chronoamperometry was conducted at the first potential when no zinc was

DOI: 10.1021/acs.jpcc.6b12036
J. Phys. Chem. C 2017, 121, 3938−3946

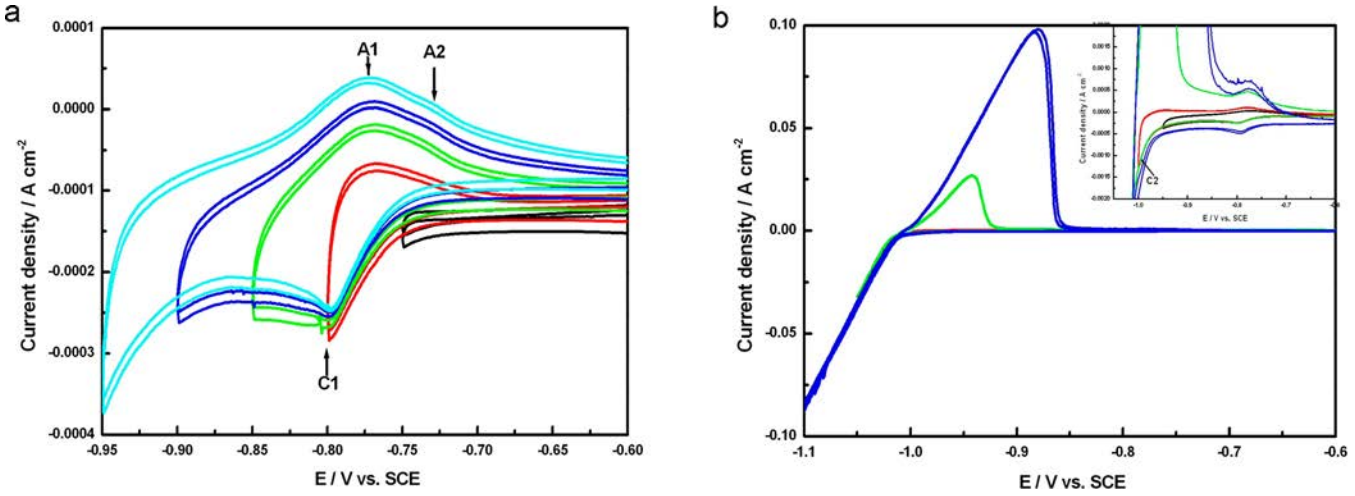

Figure 2. Successively recorded cyclic voltammograms with increasing cathodic limits from (a) −0.75 to −0.95 V vs SCE and from (b) −0.95 to −1.1 V vs SCE obtained at 10 mV s^{-1} during electrodeposition of zinc onto polycrystalline copper in a solution containing 1.0 M $ZnBr_2$. The anodic limit in all of the CVs is −0.3 V vs SCE. The inset shows a close-up of the region for small current peaks.

present on the copper surface for 20 s and by increasing (or decreasing) the potential at an interval of 0.05 V versus SCE. The time interval was 1×10^{-5} s. Chronocoulometry was carried out at the first potential when zinc was not present on the copper surface for 20 s while increasing (or decreasing) the potential at an interval of 0.05 V versus SCE. The pulse width was 0.01 s, and the time interval was 1×10^{-6} s. All of the measurements were performed at room temperature (25 °C), and the results were normalized by the footprint area.

3. RESULTS AND DISCUSSION

According to the basic nucleation and growth mechanism, a simple process consisting of three steps is proposed (Figure 1a). In the beginning, it is a Langmuir-type adsorption−desorption process (step 1), and the related current density is given by the following equation:[21−23]

$$J_{ad} = k_{ad1} \exp(-k_{ad2}t) \quad (1)$$

where t is time and $k_{ad1(2)}$ is the adjusted parameter obtained by fitting with experimental data in the potential step method. Second, two-dimensional (2D) nucleation and growth (step 2) are described as either instantaneous or progressive processes. The dissolution sites are active in the beginning of the potential step experiments in the instantaneous model, and dissolution sites become activated gradually as the experiment proceeds in the progressive model. The current densities in these two cases are[21−23]

$$J_{2DI} = k_{2DI1}t \exp(-k_{2DI2}t^2) \quad (2)$$

for the instantaneous case and

$$J_{2DP} = k_{2DP1}t^2 \exp(-k_{2DP2}t^3) \quad (3)$$

for the progressive case. $k_{2DI1(2)}$ and $k_{2DP1(2)}$ are the adjusted parameters, which can also be obtained by fitting with experimental data in the potential step method. In this case, the current density for steps 1 and 2 obey a simple exponential relationship:

$$J_n = at^n \exp(-bt^{n+1}) \quad (4)$$

where a and b are adjusted parameters, showing $n = 0$ for a Langmuir-type adsorption−desorption process, $n = 1$ for 2D nucleation and growth in the instantaneous case, and $n = 2$ for 2D nucleation and growth in the progressive case. Third, there is three-dimensional (3D) nucleation and growth (step 3), and the related current density is described by the following equation:[21−23]

$$J_{3D} = k_{3D1}t^{-1/2}[1 - \exp(-k_{3D2}\Theta(t)t)] \quad (5)$$

where $k_{3D1(2)}$ is the adjusted parameter and

$$\Theta(t) = 1 - \frac{1 - \exp(-At)}{At} \quad (6)$$

A is another adjusted parameter obtained by fitting between the theoretical and experimental data. The function $\Theta(t)$ (current density J_{3D}) approaches zero in the short time regime. With regard to the long time region, $\Theta(t)$ approaches 1, and the exponential function is equal to zero. The current density is described by the following relationship:

$$J_{3D} = k_{3D1}t^{-1/2} \quad (7)$$

Equation 7 is similar to the Cottrell equation[27] used to describe the potential step chronamperomery. The integrated current density corresponds to the charge density Q_{3D} (in unit C cm^{-2}), and the integration result of eq 7 can be expressed as

$$Q_{3D} = ct^{1/2} \quad (8)$$

where c is an adjusted parameter. Equation 8 is similar to the Anson equation[27,28] used in the chronocoulometry model under diffusion-limited conditions. It indicates that the charge density Q_{3D} obtained by the chronocoulometry method rises with time and the plot versus $t^{1/2}$ is linear. The slope (equal to 0.5) can be used to evaluate the 3D nucleation and growth process for a long testing time. In this case, integration can also be used for eq 4 to obtain the charge density Q_n (in unit C cm^{-2}), which is expressed as[29]

$$Q_n = e \exp(-ft^m) \quad (9)$$

where e and f are the adjusted parameters. It shows $m = 1$ for a Langmuir-type adsorption−desorption process adopting the

DOI: 10.1021/acs.jpcc.6b12036
J. Phys. Chem. C 2017, 121, 3938−3946

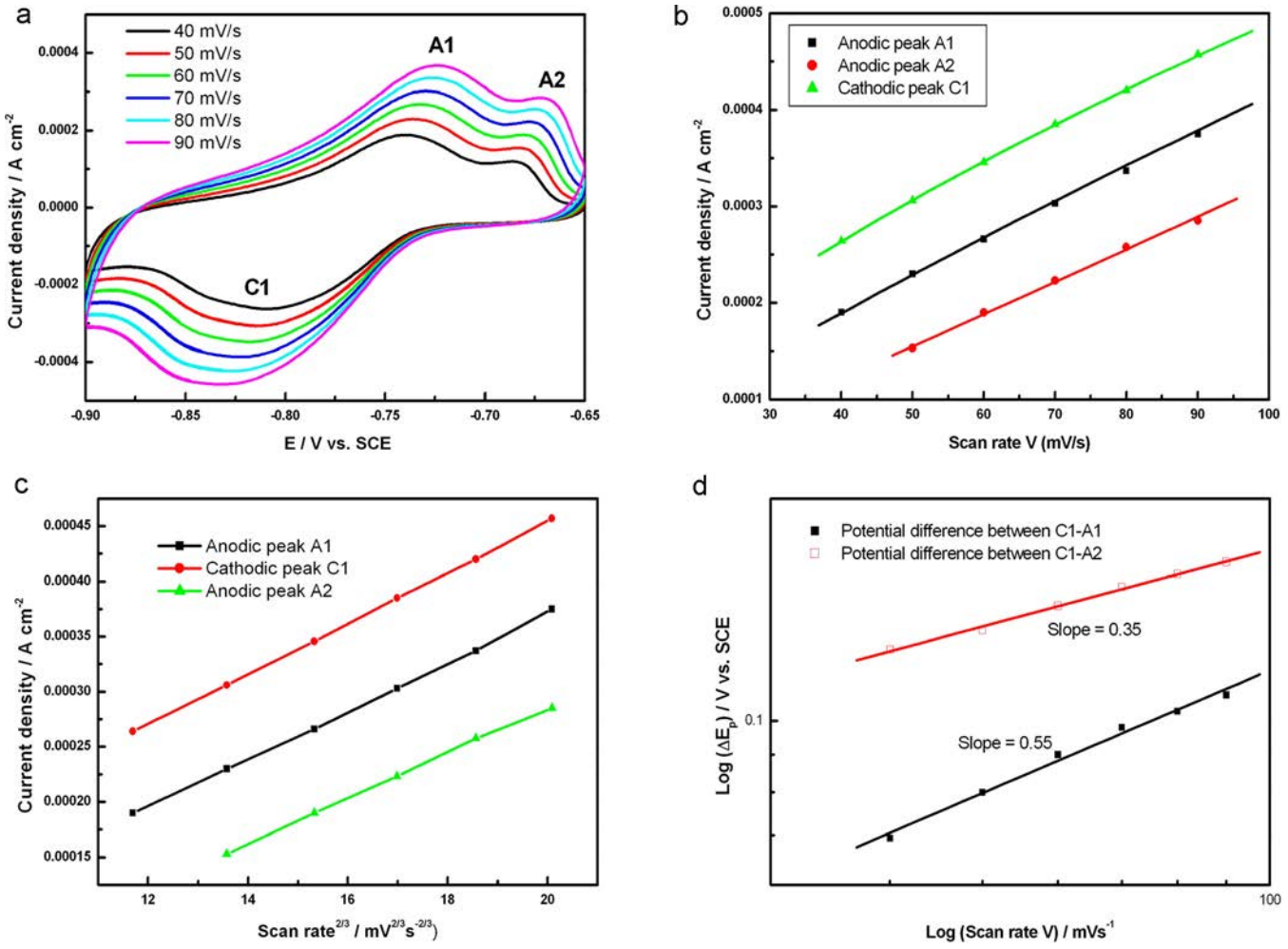

Figure 3. (a) Cyclic voltammograms in the potential range between −0.65 and −0.9 V vs SCE obtained at a scanning rate from 40 to 90 mV s^{-1} during electrodeposition of zinc on copper in 1.0 M $ZnBr_2$; (b) scanning rate and (c) 2/3 power of the scanning rate dependence in zinc underpotential deposition (C1) and desorption peaks (A1 and A2) current densities; and (d) potential difference between the anodic and cathodic peak potentials.

Bewick−Fleichman−Thirsk (BFT) nucleation growth model for the formation of monolayer adsorbed ions, m = 2 for 2D nucleation and growth in the instantaneous case, and m = 3 for 2D nucleation and growth in the progressive case. Equation 9 indicates that the charge density Q_n obtained by the chronocoulometry method goes up with time and the slope of ($\log(Q_n)$ versus $\log(t)$) is equal to the index m, which can be used to identify different nucleation and growth processes. The adsorption and 2D growth processes (steps 1 and 2) occur in the early stages (shorter time), and the contribution of the current density from 3D nucleation and growth can be neglected. However, the current density of 3D growth is the main contribution in the latter stages (longer time as shown in step 3).

To assess the different growth processes quantitatively, the current densities of different processes are calculated on the basis of eq 4 as shown in Figure 1b. The data of the 3D nucleation and growth process are also obtained from eq 7, but they are useful in the longer time case. The adjusted parameters are selected to be unity for simplicity. It can be observed that the current density is larger in the Langmuir-type adsorption−desorption process initially and the current density of the Langmuir-type adsorption−desorption process decreases for a longer time, and the current density of 2D nucleation and growth increases showing the peaks for the instantaneous case and then the progressive case. For a long testing time, the current density of the 3D diffusion-control nucleation and growth process is the main contributor due to the smaller current density from the other parts. In this case, the integrated current densities (charge densities) are shown in Figure 1c for the different nucleation and growth processes. The ($\log(Q_n)$ vs $\log(t)$) plot shows a linear relationship in the Langmuir-type adsorption−desorption process with slope 1. The 2D nucleation and growth in the instantaneous case shows slope 2, and the 2D nucleation and growth in the progressive case shows slope 3. The slope of 0.5 corresponds to the 3D nucleation and growth process under diffusion-limited conditions.

In the experimental evaluation, zinc is deposited on a polycrystalline copper substrate. The cyclic voltammograms (CV) of the Cu substrate in 1 mol L^{-1} Zn−Br solution in Figure 2a,b are acquired from −0.4 V to the potential range between −0.7 and −1.1 V vs SCE at a scanning rate 10 mV s^{-1}. With the voltage envelope extended from −0.75 to 0.95 V vs SCE as shown in Figure 2a, there is a well-defined reduced peak at about −0.8 V vs SCE in the cathode scan (C1), and there is a clear oxidation peak at about −0.75 V vs SCE (A1) and a not well-defined oxidation peak (A2) at the more positive potential

DOI: 10.1021/acs.jpcc.6b12036
J. Phys. Chem. C 2017, 121, 3938−3946

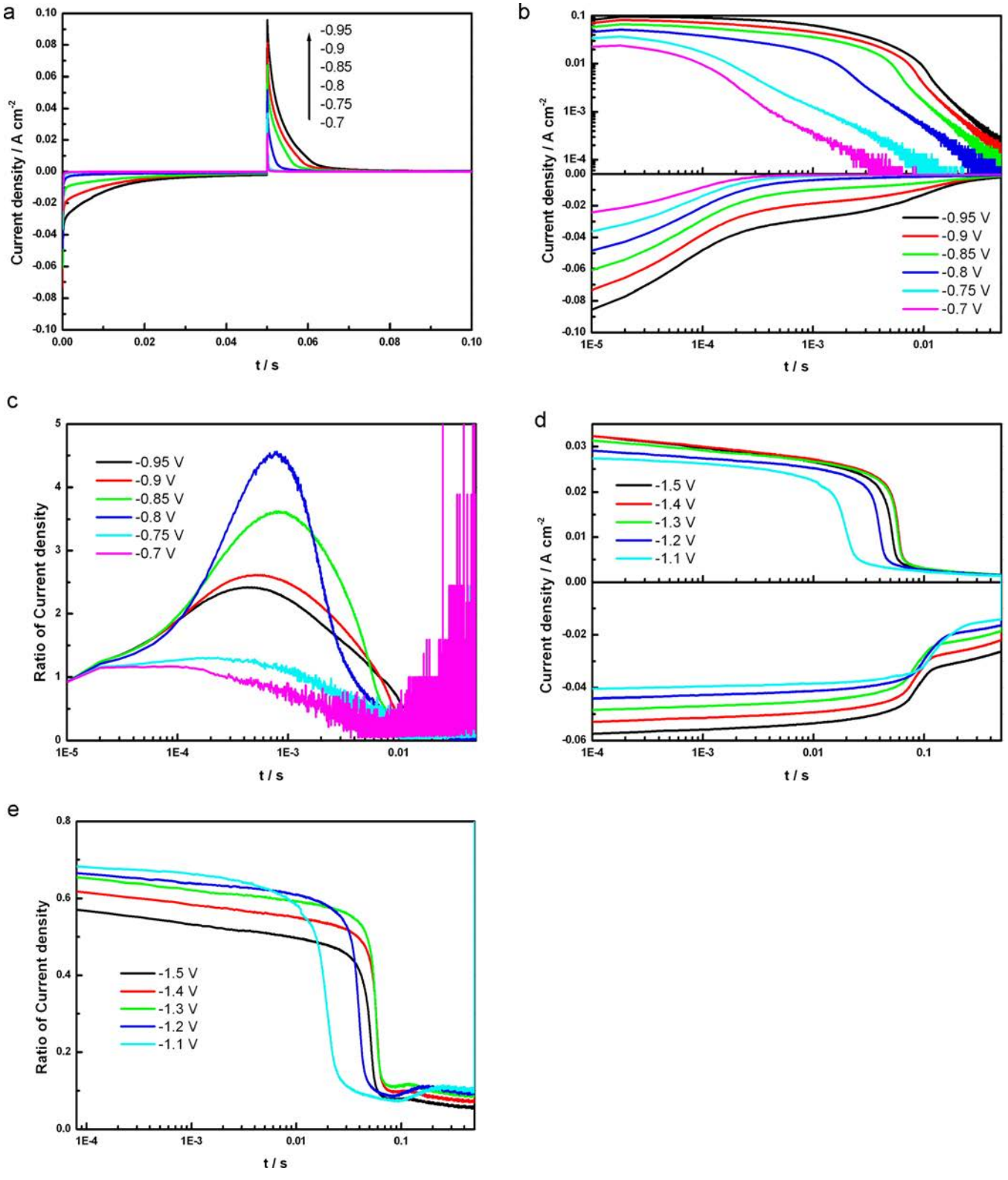

Figure 4. (a) A set of experimental current density−time transients recorded in 1.0 M $ZnBr_2$ by the double potential step technique. In all of the cases, an initial potential −0.6 V vs SCE is applied to the polycrystalline copper electrode, and the final potentials vary from −0.7 to −0.95 V vs SCE in a time interval of 1×10^{-5} s during the testing time of 0.05 s (positive steps). For $t > 0.05$ s, the related reverse potential step (negative) is also applied. (b) Related experimental current density−time transients for the positive (down) and negative (upper) potential steps. (c) Reduced current density for the ratio of the deposition and dissolution process. The current density−time transients are shown for positive (down) and negative (upper) potential steps for the overpotential deposition (OPD) case (d). (e) Reduced current density. The final potentials vary from −1.1 to −1.5 V vs SCE.

DOI: 10.1021/acs.jpcc.6b12036
J. Phys. Chem. C 2017, 121, 3938−3946

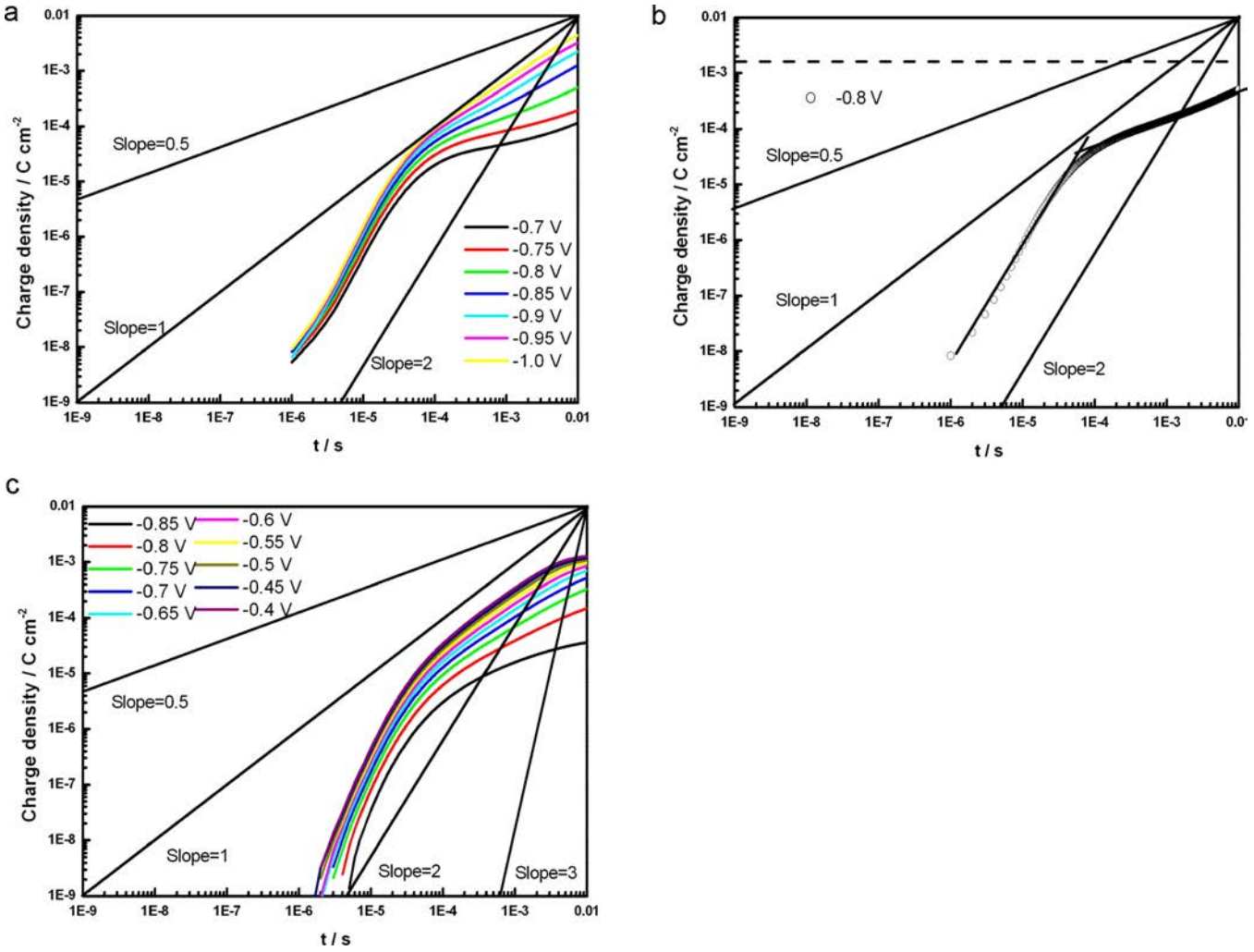

Figure 5. Typical experimental chronocoulometric data: (a) Potential of the electrodes is potentiostatically stepped from −0.6 to the final potentials varied from −0.7 to −1.0 V vs SCE in the time interval 1×10^{-6} s at a pulse width of 0.01 s; (b) chronocoulometric data for the case of the final potential −0.8 V; and (c) chronocoulometric data for potentiostatical stepping from −0.9 V to the final potentials varied from −0.8 to −0.4 V vs SCE. Solid lines with slopes of 0.5, 1, 2, and 3 are shown for comparison.

in the CV curves. At the same time, there is a shoulder C2 in the cathodic scan between −0.9 and 1.0 V vs SCE as shown in Figure 2b. As the electrode potential changes to more negative values, such as −1.1 V vs SCE, the current density increases steadily due to zinc deposition at the first negative potential in the so-called overpotential deposition (OPD) region, and then the hydrogen evolution reaction (HER) appears at a more negative potential. The inverse potential scan shows a crossover of the cathodic and anodic branches typical of the formation of a new phase involving nucleation.[21] There is a new anodic peak at −0.9 V, indicating dissolution of bulk zinc. In this case, the cathodic peak C1 at −0.8 V occurs by the underpotential deposition (UPD) process. It is because the work function of Cu is close to that of Zn, resulting in monolayer formation at the potential positive to the Nernst potential (underpotential deposition, UPD).[30,31] With regard to the monolayer, nuclei are generated, and this zinc monolayer influences the growth of subsequent layers. In this case, the cathode current shoulder C2 at the potential between −0.9 and 1.0 V vs SCE can be ascribed to Cu−Zn alloy formation in the potential region between the Nernst potential and underpotential deposition region. The two oxidation peaks A2 and A1 at about −0.73 and −0.77 V vs SCE stem from dissolution of underpotential deposited zinc and Cu−Zn alloy, respectively.

To ensure that peak C1 is actually due to underpotential deposition of zinc and that the two oxidation peaks (A1 and A2) can be attributed to the dissolution of underpotential deposited zinc and Cu−Zn alloy, respectively, Figure 3a shows the CV curves at different scanning rates ν (from 40 to 90 mV s^{-1}) in the potential region between −0.65 and −0.9 V vs SCE. There are two oxidation peaks (A1 and A2). Figure 3b shows the dependence of the valtammetric response of each peak on the scanning rate ν in the plot of log I_p versus log ν (Figure 3b). The peak current densities I_p of all three peaks are proportional to the scanning rate ν bearing a linear dependence with a slope of 0.67 for cathodic peak C1 and slope of 0.86 (1.06) for the anodic peak A1 (A2), indicating that these three peaks are associated with surface processes.[32] When the peak current densities are plotted as a function of $V^{2/3}$, the plots appear linear over the entire range of scanning rates (Figure 3c). A $\nu^{2/3}$ scanning rate dependence of the peak current density is characteristic of a two-dimensional nucleation and growth mechanism.[33] The potential difference between the oxidation and reduction peaks is defined as ΔE_p, and the plots of log ΔE_p versus log ν (Figure 3d) are also linear with slopes of 0.55

DOI: 10.1021/acs.jpcc.6b12036
J. Phys. Chem. C 2017, 121, 3938−3946

(0.35) for potential differences between the reduction peak C1 and anodic peak A1 (A2). The above slopes for peaks C1 and A2 are very close to the predicted values derived by the Sanchez−Maestre model,[33] and it can be concluded that zinc underpotential deposition on polycrystalline Cu proceeds by a two-dimensional nucleation and growth mechanism manifested by the anodic and cathodic peaks A1 and C1. The oxidation peaks A2 can be attributed to dissolution of the Cu−Zn alloy.

The kinetics and mechanism of zinc deposition on polycrystalline copper and respective dissolution are studied potentiostatically. The current density transients are measured by the double-potential step technique. The experiments involve the application of an initial potential −0.6 V to the copper electrode surface, and under these conditions, Zn deposition has not started as indicated by the voltammetric study. After application of this initial potential, the first potential step varies within the range between −0.7 and −1.0 V vs SCE and is applied to the copper electrode surface for time = 0.05 s. The final potential is in the zinc UPD region, which can monitor zinc deposition on the polycrystalline copper surface. The second potential step is the same as the initial potential. Figure 4a shows a set of experimental current density transients obtained by the double potential step technique. The shape of the transients is quite similar to those reported previously for zinc deposition on a glassy carbon electrode.[34] The current density curves increase or decrease quickly in the deposition (negative) and dissolution (positive) processes, respectively, corresponding to the small operating potential step such as −0.7 and −0.75 V vs SCE. However, for the large operating potential step from −0.8 to −0.95 V vs SCE, the current density curves increase or decrease slowly and show shoulders. It is because the polycrystalline copper substrate and the current density curves show shoulders rather than maxima as observed from single-crystal substrates.[32,34,35] To show the current density transient data clearly, especially the early stages of electrodeposition, the current density transients in the logarithmic format for the time axis are shown in Figure 4b for the deposition (down) and dissolution (upper) processes. Two distinct stairs are observed as the current densities decrease in the Zn deposition process with time. The first stair occurs at about 1.0×10^{-4} s and the second one at 2.0×10^{-2} s. The two-stair process only appears for larger potential steps such as from −0.8 to −0.95 V vs SCE, and only one stair appears for small potential steps such as potential −0.7 and −0.75 V vs SCE. In the dissolution process (upper), a larger current density and wider shoulder are observed for larger potential steps. In another case, the reduced current densities corresponding to the ratio of the related dissolution and deposition processes are shown in Figure 4c. It shows that the ratios are about unity or less than unity with time for the small potential steps, such as −0.7 and −0.75 V vs SCE. However, the ratio shows a clear peak, which approaches the maximum value of about 4.5 at 1.0×10^{-3} s for the potential step −0.8 V vs SCE. With increasing potential steps, the peak values decrease and shift to the shorter time, such as the maximum value that is about 2.2 at 5.0×10^{-4} s for the potential step −0.95 V vs SCE. If the potential step is large enough, such as a final potential being larger than −1.0 V vs SCE, the overpotential deposition process (OPD) appears as shown by the voltammetric curves. The zinc deposition process is also shown in the chronoamperommetric data (Figure 4d), and a ratio of the current density is shown in Figure 4e. The reduced current densities in the deposition and dissolution processes are less than unity in the testing time, and the larger is the electric field, the smaller is the ratio of current densities.

According to the usual description of the chronocoulometric experiments,[27] it is also sensitive to the time scale, and it may be interesting to consider the different nucleation and growth mechanisms based on the slopes according to the previous discussion. In this case, the chronocoulometric experiments are performed with a pulse width of 0.01, time interval of 1.0×10^{-6} s, and −0.6 V as the initial potential and final potential steps changing from −0.7 to −1.0 V vs SCE. Figure 5a shows the results as $\log(Q_n)$ versus $\log(t)$, and the solid lines with slopes of 0.5, 1, 2, and 3 are shown for comparison. The Langmuir-type adsorption−desorption processes appear at first at time shorter than 4.0×10^{-5} s corresponding to the slope of about unity. The adsorption process shows the larger contribution to the charge density for the low electric field cases. The 2D instantaneous nucleation and growth mechanisms are the main contributors at time shorter than 1.0×10^{-4} s corresponding to a slope of about 2. As time is increased, the slope decreases and approaches 0.5.

The chronocoulometric data for the final potential of −0.8 V are shown in Figure 5b, showing the special potential corresponding to UPD Zn. The 2D instantaneous nucleation and growth mechanisms are the main contributors corresponding to a slope of 2. However, the Langmuir-type adsorption−desorption process appears at first corresponding to a slope of less than 2, and the 2D progressive nucleation and growth mechanisms also contribute to the charge intensity at time of about 1×10^{-5} s corresponding to a slope larger than 2. The slope of 0.5 is observed for time longer than 1.0×10^{-4} s. The turning point at which the slope changes from 2 to 0.5 can be determined from the intersection between the lines with different slopes. At the turning point, the accumulated charge is about 4.2×10^{-5} C cm^{-2} at time 6.5×10^{-5} s. The accumulated charge is about 1.3×10^{14} Zn atoms per cm^2 on the copper surface, corresponding to about 0.9% surface coverage with respect to Cu surface atoms density (1.5×10^{15} atoms cm^{-2}, square (1 × 1) lattice, and atomic distance of 0.26 nm[36]). That is to say, the growth mechanism would change due to the surface coverage 0.9% of Zn on the copper substrate corresponding to the different slopes in the chronocoulometric data. As compared to the electrochemical aggregative growth model for Ag on a carbon substrate,[26] the number of large-size nanoclusters reaches saturation at a small surface coverage of about 1%, corresponding to that the Ag nucleation exclusion zones overlap and cover the entire surface. The turning point in the chronocoulometric data also corresponds to that the Zn nucleation exclusion zones overlap and cover the entire surface due to the similar surface coverage. A time of 1.0×10^{-3} s corresponds to the maximum dissolution rate as shown in Figure 4c. The accumulated charge is 1.6×10^{-4} C cm^{-2} associated with a surface coverage of 33%. Because the surface coverage is similar to that of the S monolayer on Au (111) and polycrystalline Au surface,[23] the Zn monolayer is formed at this time. On account of the formation of monolayer Zn on the surface, the ratio of the dissolution/deposition currents decreases after this time as shown in Figure 4c. The current density of the dissolution process decreases quickly after this time as shown in Figure 4b, suggesting that the 3D nucleation and growth mechanisms contribute to the accumulated charges after this stage and the slope becomes larger than 0.5 as shown by the chronocoulometric data. It also indicates that the first stair of deposition current density in Figure 4b is induced by

DOI: 10.1021/acs.jpcc.6b12036
J. Phys. Chem. C 2017, 121, 3938−3946

the 2D nucleation and growth process due to almost the same time region in the chronocoulometric data and the second stair is the mediator process between the 2D nucleation and growth mechanism and the 3D growth case, which the monolayer metal formed during the time.

A simple nucleation and growth process for zinc deposition on copper is proposed. As a small potential step (electric field) is applied to the copper surface such as the potential step for the initial potential of −0.6 and final potential of −0.7 or −0.75 V vs SCE, the limited electric field between the electrode and electrolyte reduces slightly the zinc constituent deposited on copper. Although 1% surface coverage can be reached by adsorption−desorption and 2D nucleation and growth mechanisms processes appear corresponding to the first stair in the chronoamperommetric data, the radii of the zinc islands are less than the critical radius r_C. Small-size zinc nucleation cannot form the Zn monolayer and will be stripped in the solution as they move along the surface. When the potential step is increased, for example, a final potential of −0.8 V vs SCE, the increasing zinc constituent deposited on copper leads to the formation of large zinc islands (radii larger than r_C) on the copper substrate reaching the monolayer condition (surface coverage of 33%). However, the small amount of zinc islands renders deposition of zinc to follow a two-dimensional nucleation and growth mechanism due to the larger dissolution rate of zinc under this electric field. This process can form one monolayer of zinc on the copper substrate corresponding to zinc underpotential deposition. In the larger electric field case, such as that with a final potential of −0.9 V vs SCE, the large surface coverage (about 12%) can reach easily at the turning point in the chronocoulometric data, and the accumulated charge (2.4×10^{-4} C cm^{-2}) is about 7.4×10^{14} Zn atoms per cm^2 deposited on the copper surface, which is larger than the Zn monolayer surface coverage of 33%, at the time of 5.0×10^{-4} s corresponding to the peak value in Figure 4c. Here, the deposited zinc grows along the vertical direction to form the large zinc islands, and only separated zinc particles can be found. In the OPD case, deposition of zinc mainly follows the three-dimensional nucleation and growth mechanism, and the 2D nucleation and growth process cannot be detected in the short time (less than 1.0×10^{-4} s) as shown by the chronoamperommetric data (Figure 4d,e).

The dissolution process of zinc can be assessed by the chronocoulometric experiments as shown in Figure 5c. The data are collected at a pulse of 0.01, time interval of 1.0×10^{-6} s, and −0.9 V as the initial potential. The final potential step changes from −0.85 to −0.4 V vs SCE, and the results are also shown as $\log(Q_n)$ versus $\log(t)$. The solid lines with slopes of 0.5, 1, 2, and 3 are shown for comparison. By monitoring the slope of the curves with time, it is easy to understand the dissolution process of the zinc adlayer on the copper substrate. 2D progressive nucleation appears at first at a time shorter than 1.0×10^{-5} s corresponding to a slope of 3. The slope of the curves approaches 2 before 1.0×10^{-4} s corresponding to the 2D instantaneous nucleation process. The Langmuir-type desorption processes are the main contributors because the slope is about 1 before 4.0×10^{-3} s. The 3D nucleation dissolution model under diffusion-limited conditions appears for the last time, corresponding to a slope of 0.5. The analysis is similar to that of cobalt deposition and dissolution on polycrystalline gold.[19,21] Figure 5c shows that the time region in the Langmuir-type desorption processes (slope 1) shortens with decreasing electric field, suggesting that the dissolution process is mainly determined by the desorption process of the reaction products and small electric field such as a final potential from −0.85 to −0.7 V vs SCE. The limited desorption rate of the reaction products retards the dissolution process of zinc and shows the dissolution process under diffusion-limited conditions in a short time corresponding to a slope of about 0.5 in the chronocoulometric data. In this case, the dissolution process cannot be continued. The results are also consistent with the cyclic voltammogram (CV) data, showing clear dissolution peaks of zinc at about −0.7 V vs SCE.

4. CONCLUSION

Different electrochemical methods such as cyclic voltammetry, chronoamperometry, and chronocoulometry are utilized to study the electrodeposition process of Zn on a polycrystalline cupper substrate in an aqueous solution. Chronocoulometry is a power tool to analyze the growth mechanism of metallic particles, and the different electrodeposition processes can be described by a simple exponential law related to the slopes in the chronocoulometric data. Analysis of the chronoamperometric and chronocoulometric data reveals a growth model for Zn electodeposition onto Cu with time, and a monolayer Zn deposition process is identified. The results provide a better fundamental understanding of the electrodeposition process of metallic particles and may be used to optimize electrodeposition of other metallic particles.

AUTHOR INFORMATION

Corresponding Author

*Tel.: +86 21 54342501. Fax: +86 21 54345119. E-mail: shxu@ee.ecnu.edu.cn.

ORCID

Shaohui Xu: 0000-0002-8201-0354

Notes

The authors declare no competing financial interest.

ACKNOWLEDGMENTS

This work was jointly supported by the National Natural Science Foundation of China (no. 61176108), the Science and Technology Commission of Shanghai Municipality under research grant no. 14DZ2260800, PCSIRT, the Research Innovation Foundation of ECNU (no. 78210245), and the City University of Hong Kong Strategic Research Grant (ARG) no. 7004644.

REFERENCES

(1) Metal Nanoparticles. *Synthesis, Characterization, and Applications*; Feldheim, D. L., Foss, C. A., Jr., Eds.; CRC Press, Taylor & Francis Group: New York, 2002.

(2) Burda, C.; Chen, X.; Narayanan, R.; El-Sayed, M. A. Chemistry and properties of nanocrystals of different shapes. *Chem. Rev.* **2005**, *105*, 1025−1102.

(3) Paunovic, M. *Fundamentals of Electrochemical Deposition*; Wiley-Interscience: New York, 2006.

(4) *Metallic Nanomaterials*; Kumar, Challa, S. S. R., Eds.; Wiley-VCH Verlag GmbH & Co. KGaA: Weinheim, 2009.

(5) Xia, Y.; Xiong, Y.; Lim, B.; Skrabalak, S. E. Shape-controlled synthesis of metal nanocrystals: simple chemistry meets complex physics? *Angew. Chem., Int. Ed.* **2009**, *48*, 60−103.

(6) Tian, N.; Zhou, Z. Y.; Sun, S. G.; Ding, Y.; Wang, Z. L. Synthesis of tetrahexahedral platinum nanocrystals with high-index facets and high electro-oxidation activity. *Science* **2007**, *316*, 732−735.

DOI: 10.1021/acs.jpcc.6b12036
J. Phys. Chem. C 2017, 121, 3938−3946

(7) Zhang, J.; Sasaki, K.; Sutter, E.; Adzic, R. R. Stabilization of Platinum oxygen-reduction electrocatalysts using Gold clusters. *Science* **2007**, *315*, 220−222.
(8) Ustarroz, J.; Altantzis, T.; Hammons, J. A.; Hubin, A.; Bals, S.; Terryn, H. The role of nanocluster aggregation, coalescence, and recrystallization in the electrochemical deposition of platinum nanostructures. *Chem. Mater.* **2014**, *26*, 2396−2406.
(9) Kim, Y. R.; Lai, S. C. S.; McKelvey, K.; Zhang, G.; Perry, D.; Miller, T. S.; Unwin, P. R. Nucleation and aggregative growth of Palladium nanoparticles on Carbon electrodes: Experiment and kinetic model. *J. Phys. Chem. C* **2015**, *119*, 17389−17396.
(10) Nicic, I.; Liang, J.; Cammarata, V.; Alanyalioglu, M.; Demir, U.; Shannon, C. Underpotential deposition of Te monolayers on Au surfaces from Perchloric acid solution studied by chronocoulometry and EQCM. *J. Phys. Chem. B* **2002**, *106*, 12247−12252.
(11) Zimmer, A.; Broch, L.; Boulanger, C.; Stein, N. Growth mechanism during the early stages of electrodeposition of Bismuth Telluride films. *Electrochim. Acta* **2015**, *174*, 376−383.
(12) Herrero, E.; Buller, L. J.; Abruna, H. D. Underpotential deposition at single crystal surfaces of Au, Pt, Ag and other materials. *Chem. Rev.* **2001**, *101*, 1897−1930.
(13) Scharifker, B. R.; Hills, G. Theoretical and experimental studies of multiple nucleation. *Electrochim. Acta* **1983**, *28*, 879−889.
(14) Scharifker, B. R.; Mostany, J.; Palomar-Pardave, M.; Gonzalez, I. On the theory of the potentiostatic current transient for diffusion-Controlled three-dimensional electrocrystallization processes. *J. Electrochem. Soc.* **1999**, *146*, 1005−1012.
(15) Palomar-Pardave, M.; Scharifker, B. R.; Arce, E. M.; Romero-Romo, M. Nucleation and diffusion-controlled growth of electroactive centers. *Electrochim. Acta* **2005**, *50*, 4736−4745.
(16) Milchev, A.; Heerman, L. Electrochemical nucleation and growth of nano- and microparticles: some theoretical and experimental aspects. *Electrochim. Acta* **2003**, *48*, 2903−2913.
(17) Heerman, L.; Tarallo, A. Theory of the chronoamperometric transient for electrochemical nucleation with diffusion-controlled growth. *J. Electroanal. Chem.* **1999**, *470*, 70−76.
(18) Hyde, M. E.; Compton, R. G. A review of the analysis of multiple nucleation with diffusion controlled growth. *J. Electroanal. Chem.* **2003**, *549*, 1−12.
(19) Palomar-Pardave, M.; Gonzalez, I.; Batina, N. New Insights into evaluation of kinetic parameters for potentiostatic metal deposition with underpotential and overpotential deposition processes. *J. Phys. Chem. B* **2000**, *104*, 3545−3555.
(20) Lai, S. C. S.; Lazenby, R. A.; Kirkman, P. M.; Unwin, P. R. Nucleation, aggregative growth and detachment of metal nanoparticles during electrodeposition at electrode surfaces. *Chem. Sci.* **2015**, *6*, 1126−1138.
(21) Mendoza-Huizar, L. H.; Robles, J.; Palomar-Pardave, M. Nucleation and growth of cobalt onto different substrates: Part I. Underpotential deposition onto a gold electrode. *J. Electroanal. Chem.* **2002**, *521*, 95−106.
(22) Mendoza-Huizar, L. H.; Robles, J.; Palomar-Pardave, M. Nucleation and growth of cobalt onto different substrates: Part II. The UPD-OPD transition onto a gold electrode. *J. Electroanal. Chem.* **2003**, *545*, 39−45.
(23) Alanyahoglu, M.; Cakal, H.; Ozturk, A. E.; Demir, U. Electrochemical studies of the effects of pH and the surface structure of Gold substrates on the underpotential deposition of Sulfur. *J. Phys. Chem. B* **2001**, *105*, 10588−10593.
(24) Ustarroz, J.; Gupta, U.; Hubin, A.; Bals, S.; Terryn, H. Electrodeposition of Ag nanoparticles onto carbon coated TEM grids: a direct approach to study early stages of nucleation. *Electrochem. Commun.* **2010**, *12*, 1706−1709.
(25) Ustarroz, J.; Ke, X.; Hubin, A.; Bals, S.; Terryn, H. New insights into the early stages of nanoparticle electrodeposition. *J. Phys. Chem. C* **2012**, *116*, 2322−2329.
(26) Ustarroz, J.; Hammons, J. A.; Altantzis, T.; Hubin, A.; Bals, S.; Terryn, H. A generalized electrochemical aggregative growth mechanism. *J. Am. Chem. Soc.* **2013**, *135*, 11550−11561.
(27) Bard, A. J.; Larry, R. *Electrochemical Methods: Fundamentals and Applications*; John Wiley & Sons Inc.: New York, 2001.
(28) Lindström, H.; Södergren, S.; Solbrand, A.; Rensmo, H.; Hjelm, J.; Hagfeldt, A.; Lindquist, S. T. Li^+ Ion insertion in TiO_2 (Anatase). 1. Chronoamperometry on CVD films and nanoporous films. *J. Phys. Chem. B* **1997**, *101*, 7710−7716.
(29) Xu, S.; Zhu, Y.; Xiong, D.; Zhang, W.; Wang, L.; Yang, P.; Chu, Paul K. Electrochemical analysis of interface adsorption phenomena on three-dimensional nano-nickel electrode deposited on silicon microchannel plate. *Electrochim. Acta* **2016**, *194*, 253−262.
(30) Zhang, L.; Cheng, J.; Yang, Y.; Wen, Y.; Wang, X.; Cao, G. Study of zinc electrodes for single flow zinc/nickel battery application. *J. Power Sources* **2008**, *179*, 381−387.
(31) Chu, M. G.; McBreen, J.; Adzic, G. Substrate effects on Zinc deposition from Zincate solutions: I. Deposition on Cu, Au, Cd and Zn. *J. Electrochem. Soc.* **1981**, *128*, 2281−2286.
(32) Zhu, W.; Yang, J. Y.; Zhou, D. X.; Bao, S. Q.; Fan, X. A.; Duan, X. K. Electrochemical characterization of the underpotential deposition of tellurium on Au electrode. *Electrochim. Acta* **2007**, *52*, 3660−3666.
(33) Maestre, M. S.; Rodriguez-Amaro, R.; Munoz, E.; Ruiz, J. J.; Camacho, L. Use of cyclic voltammetry for studying two-dimensional phase transitions: Behaviour at low scan rates. *J. Electroanal. Chem.* **1994**, *373*, 31−37.
(34) Beshore, A. C.; Flori, B. J.; Schade, G.; O'Keefe, T. J. Nucleation and growth of zinc electrodeposited from acidic zinc solutions. *J. Appl. Electrochem.* **1987**, *17*, 765−772.
(35) Monzon, Lorena M. A.; Klodt, L.; Coey, J. M. D. Nucleation and electrochemical growth of Zinc crystals on polyaniline films. *J. Phys. Chem. C* **2012**, *116*, 18308−18317.
(36) Kim, Y.-G.; Baricuatro, J. H.; Javier, A.; Gregoire, J. M.; Soriaga, M. P. The evolution of the polycrystalline copper surface, First to Cu(111) and Then to Cu(100), at a fixed CO_2RR potential: A study by Operando EC-STM. *Langmuir* **2014**, *30*, 15053−15056.

DOI: 10.1021/acs.jpcc.6b12036
J. Phys. Chem. C 2017, 121, 3938−3946